A Dynamic Model for Microstrip–Slotline Transition and Related Structures

HUNG-YU YANG, STUDENT MEMBER, IEEE, AND NICÓLAOS G. ALEXÓPOULOS, FELLOW, IEEE

Abstract—An analysis of microstrip to slotline transition is presented. The method of moments is applied to the coupled integral equations. In the formulation, the Green's function for the grounded dielectric substrate, which takes into account all the radiation, surface wave, and substrate effects, is used. Meanwhile, all the mutual coupling effects are included in the method of moments solution. Certain related structures, such as slotline and microstrip discontinuities, a slot fed by a microstrip line, and a printed strip dipole fed by a slotline, can also be solved with this analysis. The present approach may find applications to other related transitions in MIC design.

I. Introduction

QUASI-STATIC METHODS, equivalent waveguide models, and equivalent circuit models have been widely used in the modeling of microstrip or slot type discontinuities in microwave and millimeter-wave devices in the past [1]. Recently, a more rigorous approach, which takes into account all the physical effects including radiation and surface waves, has been applied to certain microstrip discontinuities [2]–[5]. In this scheme, the method of moments, which determines the current on the strip or electric field on the slot, is implemented in the solution of the Pocklington integral equation. The exact Green's function for a grounded dielectric substrate due to either an electric dipole or a magnetic dipole has been used, which includes all the physical effects. Based on this approach, a dynamic model for microstrip–slotline transition and its related structures such as a microstrip-fed slot and a slotline-fed printed dipole is proposed in this paper. The developed model with some modifications can be applied to other types of transitions in MIC and MMIC design.

In microstrip–slotline transition, a short-circuit slotline which is etched on one side of the substrate is crossed at a right angle by an open-circuit microstrip on the opposite side. This type of transition makes the two-level circuit design possible [1]. Some experimental work has been reported in [6], [7] and a transmission line circuit model was reported in [8]. In the present approach, the radiation and surface waves due to the cross-junction, the line discontinuities, and all the mutual coupling due to the dominant mode as well as higher order modes of each line are included in the method of moments solution. The VSWR and input impedance of the transition can be determined by the current distribution on the microstrip line in conjunction with transmission line theory. One of the main features of the present method is the modeling of two coupled half-infinite lines where expansion modes are composed of piecewise-sinusoidal modes and traveling-wave and standing-wave modes. In the formulation procedure, certain important problems in MIC, MMIC, or printed antenna design can also be solved. When only one of the lines is discussed, the present approach is simplified to the modeling of slotline or microstrip line discontinuities as reported in [2]–[5]. If one of the lines is of finite length, then the method presented herein can be applied to the modeling of microstrip line-fed slot or slotline-fed printed strip dipole.

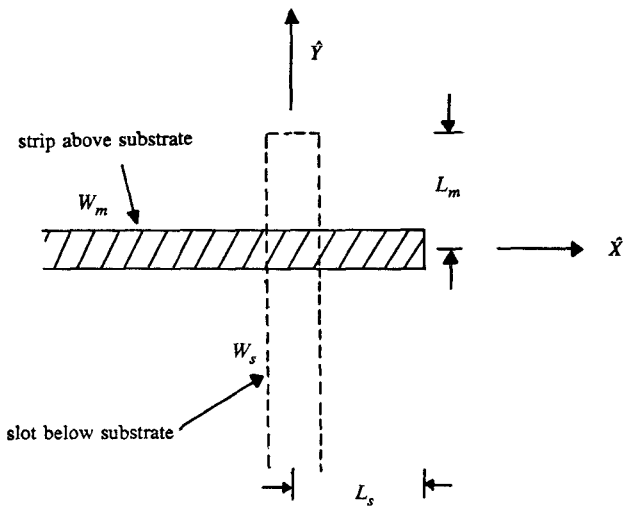

Fig. 1. Top view of microstrip–slotline transition.

II. Theory

A. Green's Function Formulation

The microstrip to slotline transition is shown in Fig. 1 and the cross section is shown in Fig. 2, where the lines are extended a certain distance beyond the cross-junction, so that their extension may act as a tuning stub. Due to the fact that the width of the lines is assumed to be much smaller than the wavelength, the transverse vector components (J_y and M_{mx}) on the lines are a second-order effect, and are neglected for simplicity. Therefore, only the $\hat{x}$-directed electric surface current J_x on the strip and the

Manuscript received March 30, 1987; revised September 3, 1987. This work was supported in part by the U.S. Army Research Office under Contract DAAG 03-83-k-0090 and in part by TRW-Micro E56129R85S.

The authors are with the Electrical Engineering Department, University of California, Los Angeles, CA 90024.

IEEE Log Number 8717988.

0018-9480/88/0200-0286$01.00 ©1988 IEEE

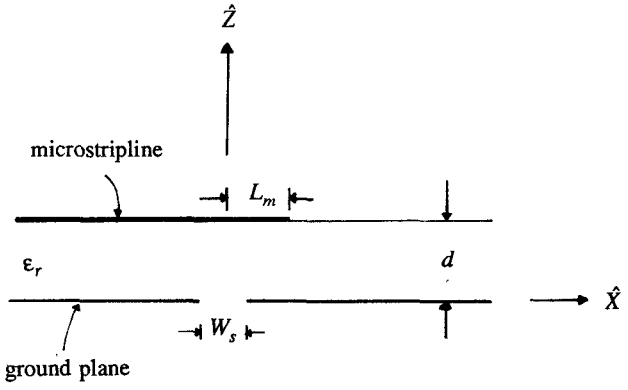

Fig. 2. Cross section of microstrip–slotline transition.

$\hat{y}$-directed magnetic surface current M_{my} ($\hat{x}$-directed electric field E_x) are considered. Under the above assumptions, the coupled integral equations can be formulated in terms of E_x and H_y. As a result, the electric field E_x at (x, y, d) due to the presence of both strip and slot is

$$E_x = \iint G_{xx} J_x \, ds_m + \iint G_{xy} M_{my} \, ds_s, \tag{1a}$$

and the difference of the magnetic field H_y at $(x, y, 0^+)$ and at $(x, y, 0^-)$ is

$$\Delta H_y = \iint G_{yx} J_x \, ds_m + \iint G_{yy} M_{my} \, ds_s, \tag{1b}$$

where G_{xx} and G_{yx} are the dyadic Green's function components due to an $\hat{x}$-directed infinitesimal electric dipole at $z = d$, and G_{xy} and G_{yy} are the dyadic Green's function components due to a $\hat{y}$-directed infinitesimal magnetic dipole at $z = 0$. J_x is the current on the microstrip s_m while M_{my} is the magnetic current (electric field) on the slotline s_s. The dyadic Green's function components G_{xx}, G_{xy}, G_{yx}, and G_{yy} can be obtained by solving the boundary value problem. The results when transformed into the spectral domain can be expressed as

$$G_{xx}(x, y|x_0, y_0) = \iint_{-\infty}^{\infty} \bar{G}_{xx}(\lambda_x, \lambda_y) e^{j\lambda_x (x - x_0)} \cdot e^{j\lambda_y (y - y_0)} \, d\lambda_x \, d\lambda_y \tag{2a}$$

$$G_{xy}(x, y|x_0, y_0) = \iint_{-\infty}^{\infty} \bar{G}_{xy}(\lambda_x, \lambda_y) e^{j\lambda_x (x - x_0)} \cdot e^{j\lambda_y (y - y_0)} \, d\lambda_x \, d\lambda_y \tag{2b}$$

$$G_{yx}(x, y|x_0, y_0) = -G_{xy}(x, y|x_0, y_0) \tag{2c}$$

and

$$G_{yy}(x, y|x_0, y_0) = \iint_{-\infty}^{\infty} \bar{G}_{yy}(\lambda_x, \lambda_y) e^{j\lambda_x (x - x_0)} \cdot e^{j\lambda_y (y - y_0)} \, d\lambda_x \, d\lambda_y \tag{2d}$$

where

$$\bar{G}_{xx}(\lambda_x, \lambda_y) = \frac{-jZ_0}{4\pi^2 k_0 \epsilon_r} \cdot \left[\frac{k_1^2 - \lambda_x^2}{D_e(\lambda)} + \frac{\lambda_x^2 q_1 (1 - \epsilon_r) \sinh(q_1 d)}{D_e(\lambda) D_m(\lambda)} \right] \sinh(q_1 d) \tag{3a}$$

$$\bar{G}_{xy}(\lambda_x, \lambda_y) = \frac{-1}{4\pi^2} \cdot \left[\frac{q_1}{D_e(\lambda)} + \frac{\lambda_x^2 (\epsilon_r - 1) \sinh(q_1 d)}{D_e(\lambda) D_m(\lambda)} \right] \tag{3b}$$

$$\bar{G}_{yy}(\lambda_x, \lambda_y) = \frac{-j}{4\pi^2 Z_0 k_0} \cdot \left[\left(k_1^2 - \lambda_y^2\right) \cdot \frac{q_1 \cosh(q_1 d) + \epsilon_r q \sinh(q_1 d)}{q_1 D_m(\lambda)} + \frac{\lambda_y^2 q (1 - \epsilon_r)}{D_e(\lambda) D_m(\lambda)} + \frac{\left(k_0^2 - \lambda_y^2\right)}{q} \right] \tag{3c}$$

$$D_e(\lambda) = q \sinh(q_1 d) + q_1 \cosh(q_1 d)$$

$$D_m(\lambda) = q_1 \sinh(q_1 d) + \epsilon_r q \cosh(q_1 d)$$

$$q = \sqrt{\lambda^2 - k_0^2}$$

$$q_1 = \sqrt{\lambda^2 - k_1^2}$$

$$\lambda = \sqrt{\lambda_x^2 + \lambda_y^2}$$

$$k_0 = \omega \sqrt{\mu_0 \epsilon_0}$$

$$k_1 = \omega \sqrt{\mu_0 \epsilon_0 \epsilon_r}$$

$$Z_0 = \sqrt{\mu_0 / \epsilon_0}. \tag{3d}$$

The integrands of (2a)–(2d) have poles whenever $D_e(\lambda)$ and/or $D_m(\lambda)$ become zero. The zeros of $D_e(\lambda)$ correspond to TE surface waves, while the zeros of $D_m(\lambda)$ correspond to TM surface waves [9]. The existence of these poles causes some problems in numerical integration. An efficient way of evaluating this type of integral is by a pole extraction technique, according to which the pole behavior is extracted out of the integrand, leaving a continuous function which may be integrated directly [10], [11]. The integrations in (2a)–(2d) may further be converted into polar coordinates such that a double infinite integration may be reduced to a finite and an infinite one.

B. The Choice of Expansion Modes

In the method of moments procedure, the J_x and M_{my} are expanded in terms of a set of known functions. The transverse dependence of J_x and M_{my} is assumed to be Maxwell's distribution, that is,

$$J_x = f(x) \cdot J_t(y)$$

and

$$M_{my} = g(y) \cdot M_t(x) \tag{4}$$

with

$$J_t(y) = \frac{1}{\pi W_m/2\sqrt{1-\left(\dfrac{y}{W_m/2}\right)^2}}$$

and

$$M_t(x) = \frac{1}{\pi W_s/2\sqrt{1-\left(\dfrac{x}{W_s/2}\right)^2}}$$

such that the edge condition is satisfied. For the transition under consideration, the modeling of two half-infinite lines is necessary, in which several mechanisms are possible. If subsectional expansion modes are used in the two finite lines with a δ gap source, then in order to characterize the cross-junction of this resonator, two sets of wave amplitudes on each line, corresponding to two different lengths of the parasitic line, are required. This scattering matrix formulation is found here to be very sensitive to error. A more reliable method is to simulate the physical situation where both the microstrip line and the slotline are terminated by a matched load. In this scheme, subsection expansion modes are used in both lines near the cross-junction region, while entire domain traveling waves are used to represent the transmitted wave in the parasitic line (slotline here) and the incident wave and the reflected wave on the feed line (microstrip line here). This method is similar to that proposed in [4], where only microstrip discontinuities are considered. Other choices of expansion modes are also possible, such as using subsectional basis functions in the feed line and subsectional modes and traveling-wave modes in the parasitic line, or the traveling-wave modes starting away from the cross-junction, such that the mutual coupling of traveling wave and PWS modes on different lines is negligible. These types of expansion modes have some advantages in the numerical analysis and will be discussed in the next section.

The traveling-wave mode used in the expansion function corresponds to the fundamental propagating mode of the microstrip line or the slotline. The microstrip line and slotline propagation constants k_m and k_s, respectively, can be obtained through the following characteristic equations [4] and [5]:

$$\int_{-\infty}^{\infty} \bar{G}_{xx}(k_m, \lambda_y) F_y^2(\lambda_y)\, d\lambda_y = 0 \tag{5a}$$

$$\int_{-\infty}^{\infty} \bar{G}_{yy}(\lambda_x, k_s) F_x^2(\lambda_x)\, d\lambda_x = 0 \tag{5b}$$

where

$$F_y(\lambda_y) = J_0(\lambda_y W_m/2) \tag{6a}$$

and

$$F_x(\lambda_x) = J_0(\lambda_x W_s/2). \tag{6b}$$

From the information of k_m and k_s, the unknown current distribution on the microstrip line can be expanded as

$$f(x) = I^{\text{inc}} + I^{\text{ref}} + \sum_{n=1}^{N} I_n f_n(x) \tag{7}$$

while the unknown electric field distribution in the slotline can be expanded as

$$g(y) = V^t + \sum_{n=1}^{M} E_n g_n(y) \tag{8}$$

where

$$I^{\text{inc}} = e^{-jk_m x} \tag{9a}$$

$$I^{\text{ref}} = -\Gamma e^{jk_m x} \tag{9b}$$

and

$$V^t = Te^{jk_s y}. \tag{9c}$$

Piecewise-sinusoidal (PWS) modes are used as subsectional expansion modes and are defined starting from the end of each line. These modes are defined as

$$f_n(x) = \frac{\sin k_e(h - |x + nh|)}{\sin k_e h}$$

$$\text{for } |x + nh| < h, \quad |y| < W_m/2 \tag{10a}$$

and

$$g_n(y) = \frac{\sin k_e(h - |y + nh|)}{\sin k_e h}$$

$$\text{for } |y + nh| < h, \quad |x| < W_s/2 \tag{10b}$$

where h is the half-length of the PWS mode. The choice of k_e can be quite arbitrary. Here k_e is chosen as $\sqrt{(\epsilon_r + 1)/2}\, k_0$ such that it is close to its physical value and it facilitates the numerical integration when the asymptotic extraction technique is applied [12].

C. The Method of Moments and Matrix Formulation

The coupled integral equations can be obtained from (1a) and (1b) by forcing the boundary conditions that the E-field must be zero on the microstrip line and the H-field must be continuous across the slotline. When the expansion modes are substituted into (1a) and (1b),

$$\iint \left[I^{\text{inc}} + I^{\text{ref}} + \sum_{n=1}^{N} I_n f_n \right] J_t(y_0) G_{xx}(x, y|x_0, y_0)\, dx_0\, dy_0$$

$$+ \iint \left[V^t + \sum_{n=1}^{M} E_n g_n \right] M_t(x_0) G_{xy}(x, y|x_0, y_0)\, dx_0\, dy_0 = 0 \tag{11}$$

is obtained for each (x, y) on the microstrip line and

$$\iint\left[I^{\text{inc}}+I^{\text{ref}}+\sum_{n=1}^{N} I_n f_n\right] J_t(y_0) G_{yx}(x, y|x_0, y_0)\, dx_0\, dy_0 + \iint\left[V^t+\sum_{n=1}^{M} E_n g_n\right] M_t(x_0) G_{yy}(x, y|x_0, y_0)\, dx_0\, dy_0 = 0 \quad (12)$$

is obtained for every (x, y) in the slotline.

In (11) and (12), there are $M+N+2$ unknowns. In Galerkin's procedure, $N+1$ PWS testing functions on the microstrip line are applied to (11), while $M+1$ PWS testing functions in the slotline are applied to (12), to obtain $M+N+2$ linear equations with $M+N+2$ unknowns which, when expressed in matrix form, are

$$\begin{bmatrix} [Z_{\text{self}}] & [Z_{\text{tself}}] & [T_{\text{meact}}] & [T_{\text{tmeact}}] \\ [T_{\text{emact}}] & [T_{\text{temact}}] & [Y_{\text{self}}] & [Y_{\text{tself}}] \end{bmatrix} \begin{bmatrix} [I] \\ -\Gamma \\ [E] \\ T \end{bmatrix} = \begin{bmatrix} [I_{\text{inc}}] \\ [V_{\text{tra}}] \end{bmatrix} \quad (13)$$

where $[Z_{\text{self}}]$ is an $(N+1)\times N$ matrix with matrix elements

$$Z_{\text{self}}^{nm} = \iint_{-\infty}^{\infty} \bar{G}_{xx}(\lambda_x, \lambda_y) F_y^2(\lambda_y) A^2(\lambda_x) \cdot \cos\left[\lambda_x(m-n)h\right] d\lambda_x d\lambda_y \quad (14)$$

$[Z_{\text{tself}}]$ is an $(N+1)\times 1$ column vector with elements

$$Z_{\text{tself}}^{n} = \iint_{-\infty}^{\infty} \bar{G}_{xx}(\lambda_x, \lambda_y) F_y^2(\lambda_y) P(\lambda_x) \cdot A(\lambda_x) e^{jnh\lambda_x} d\lambda_x d\lambda_y \quad (15)$$

$[Y_{\text{self}}]$ is an $(M+1)\times M$ matrix with matrix elements

$$Y_{\text{self}}^{mn} = \iint_{-\infty}^{\infty} \bar{G}_{yy}(\lambda_x, \lambda_y) F_x^2(\lambda_x) A^2(\lambda_y) \cdot \cos\left[\lambda_y(m-n)h\right] d\lambda_x d\lambda_y \quad (16)$$

$[Y_{\text{tself}}]$ is an $(M+1)\times 1$ column vector with elements

$$Y_{\text{tself}}^{m} = \iint_{-\infty}^{\infty} \bar{G}_{yy}(\lambda_x, \lambda_y) F_x^2(\lambda_x) Q(\lambda_y) \cdot A(\lambda_y) e^{jmh\lambda_y} d\lambda_x d\lambda_y \quad (17)$$

$[T_{\text{meact}}]$ is an $(N+1)\times M$ matrix with matrix elements

$$T_{\text{meact}}^{nm} = \iint_{-\infty}^{\infty} \bar{G}_{xy}(\lambda_x, \lambda_y) F_x(\lambda_x) F_y(\lambda_y) A(\lambda_x) A(\lambda_y) \cdot \cos\left[\lambda_x(L_m - nh)\right] \cos\left[\lambda_y(L_s - mh)\right] d\lambda_x d\lambda_y \quad (18)$$

$[T_{\text{emact}}]$ is an $(M+1)\times N$ matrix with matrix elements

$$T_{\text{emact}}^{mn} = -T_{\text{meact}}^{nm} \quad (19)$$

$[T_{\text{tmeact}}]$ is an $(N+1)\times 1$ column vector with elements

$$T_{\text{tmeact}}^{n} = \iint_{-\infty}^{\infty} \bar{G}_{xy}(\lambda_x, \lambda_y) F_x(\lambda_x) F_y(\lambda_y) Q(\lambda_y) A(\lambda_x) \cdot \cos\left[\lambda_x(L_m - nh)\right] e^{j\lambda_y L_s} d\lambda_x d\lambda_y \quad (20)$$

$[T_{\text{temact}}]$ is an $(M+1)\times 1$ column vector with elements

$$T_{\text{temact}}^{m} = \iint_{-\infty}^{\infty} \bar{G}_{yx}(\lambda_x, \lambda_y) F_x(\lambda_x) F_y(\lambda_y) P(\lambda_x) A(\lambda_y) \cdot \cos\left[\lambda_y(L_s - mh)\right] e^{j\lambda_x L_m} d\lambda_x d\lambda_y \quad (21)$$

$[V_{\text{tra}}]$ is an $(M+1)\times 1$ column vector with elements

$$V_{\text{tra}}^{m} = -\iint_{-\infty}^{\infty} \bar{G}_{yx}(\lambda_x, \lambda_y) F_x(\lambda_x) F_y(\lambda_y) R(\lambda_x) A(\lambda_y) \cdot \cos\left[\lambda_y(L_s - mh)\right] e^{j\lambda_x L_m} d\lambda_x d\lambda_y \quad (22)$$

$[I_{\text{inc}}]$ is an $(N+1)\times 1$ column vector with elements

$$I_{\text{inc}}^{n} = -\iint_{-\infty}^{\infty} \bar{G}_{xx}(\lambda_x, \lambda_y) F_y^2(\lambda_y) R(\lambda_x) \cdot A(\lambda_x) e^{jnh\lambda_x} d\lambda_x d\lambda_y \quad (23)$$

$$A(x) = 2k_e \frac{(\cos k_e h - \cos xh)}{(x^2 - k_e^2)} \quad (24)$$

$$P(\lambda_x) = \left[e^{(-j\lambda_x k_m/2k_e)} + j\right] \int_{-\infty}^{0} \sin k_m x e^{j\lambda_x x}\, dx \quad (25)$$

$$Q(\lambda_y) = \left[e^{(-j\lambda_y k_s/2k_e)} + j\right] \int_{-\infty}^{0} \sin k_s y e^{j\lambda_y y}\, dy \quad (26)$$

$$R(\lambda_x) = \left[e^{(-j\lambda_x k_m/2k_e)} - j\right] \int_{-\infty}^{0} \sin k_m x e^{j\lambda_x x}\, dx. \quad (27)$$

$[I]$ is an $(N)\times 1$ column vector with elements $I_1, I_2, \cdots, I_N$; $[E]$ is an $(M)\times 1$ column vector with elements $E_1, E_2, \cdots, E_M$; and L_s and L_m are the stub length for slotline and microstrip, respectively.

D. Some Aspects in Numerical Analysis

The numerical integrations in (14)–(23) are computed after transforming into polar coordinates. The convergence of the integrations depends mainly upon the Green's function. Since $\bar{G}_{xy}(\lambda_x, \lambda_y)$ or $\bar{G}_{yx}(\lambda_x, \lambda_y)$ decays exponentially, with the decay factor proportional to the thickness of the substrate, (18)–(22) are integrated directly. The integrands in (14)–(17) and (23) are slowly convergent. Therefore the asymptotic extraction technique [12] is applied, which requires additional computations of the self and mutual reactions of the PWS and traveling-wave modes in homogeneous medium with $\epsilon_{\text{eff}} = \sqrt{(\epsilon_r+1)/2}$.

Because of the method of numerical integration in (14)–(23), it is convenient to deal with real expansion modes; therefore the traveling-wave mode is usually decomposed into sine and cosine terms [4]. Also, since the current or electric field is zero at the end of the lines, the

cosine expansion mode starts a quarter wavelength from the terminated end.

The formulation in the last section is quite flexible and can be easily modified to other types of mode expansion mechanisms. For example, the traveling-wave modes may start more than a wavelength away from the cross-junction, which modifies the Fourier transform of the traveling-wave mode in the above formulation. This type of expansion mode has the advantage that the mutual coupling between traveling-wave modes and PWS modes of the other line ($[T_{\text{temact}}]$ and $[T_{\text{tmeact}}]$) is negligible. Therefore, the computation effort in (13) can be reduced. Besides, the solutions are automatically convergent in the sense of the number of expansion modes. Another type of expansion mode is also possible where only PSW modes are used in the feed line. This has the advantage of providing some insight into the current distribution on the feed line and of avoiding the computations of the submatrices $[Y_{\text{tself}}]$ and $[T_{\text{tmeact}}]$ in (13). The above different mode expansion mechanisms may also be used to check the convergence and stability of the solution.

E. Related Problems

Each submatrix itself in (13) has a physical meaning, which contains the information of the self-reaction or mutual coupling of different expansion modes. With submatrices $[Z_{\text{self}}]$, $[Z_{\text{tself}}]$, and $[I_{\text{inc}}]$, the end effects of an open-circuit microstrip line can be determined, while with $[Y_{\text{self}}]$, $[Y_{\text{tself}}]$, and $[V_{\text{inc}}]$ (determined in a way similar to $[I_{\text{inc}}]$) the end effects of a short-circuit slotline can be determined. Also, if the parasitic line (either slotline or microstrip line) is finite where only PWS modes are used, the problems of the microstrip-line-fed slot or the slotline-fed printed strip dipole can be solved with this model.

III. Numerical Results

A. Microstrip–Slotline Transition

The results of microstrip–slotline transition are obtained based on the developed algorithm. The numerical analysis is performed on the IBM 3090 system. Typically, for each datum it takes about one minute and thirty seconds of computer time, in contrast to a half second, to obtain the propagation constant k_m, although a lot of effort has been made to reduce the computer cost. An example of a 50-Ω microstrip line to an 80-Ω slotline transition is given. The results of the VSWR and input impedance are shown in Figs. 3 and 4, respectively. The results of VSWR are first checked by interchanging the feed line and the parasitic line. The differences in $|\Gamma|$ are within 2 percent, which is consistent with the property of low-loss two-port networks. The obtained complex reflection coefficient is further checked by changing the number of modes and different mode expansion mechanisms as described in the last section. Two sets of input impedances with different numbers of expansion modes and base function size are shown in

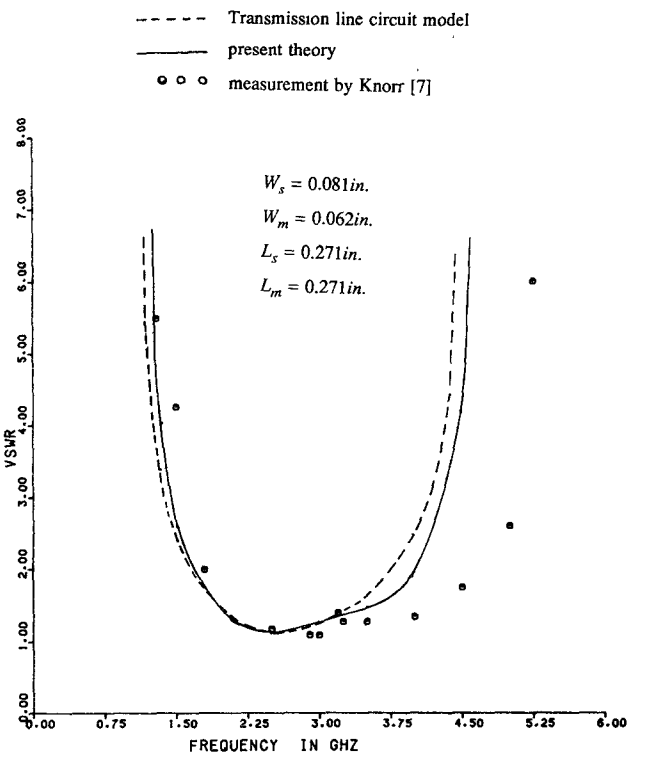

Fig. 3. VSWR versus frequency for microstrip–slotline transition. ϵ_r = 20 and d = 0.125 in.

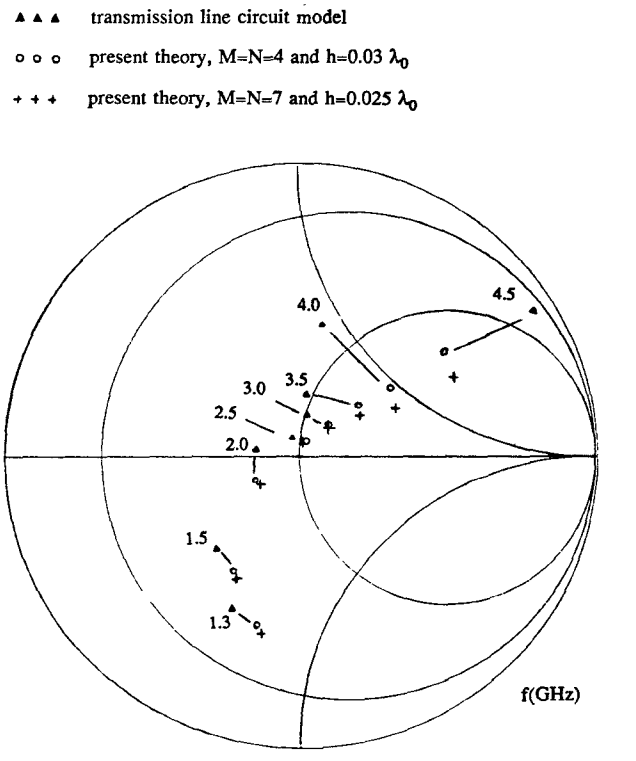

Fig. 4. Smith chart plot of impedance versus frequency for microstrip–slotline transition. The reference plane is on the center of the cross section.

Fig. 4 to illustrate a convergence test example. With the particular device parameters it is found that both the magnitude and the phase of the reflection coefficient converge very well (2 percent in $|\Gamma|$ and 5° in phase) for $d \leqslant 0.036\lambda_0$. However, for higher frequencies, the results are more unstable, and typically the results are 5–10 percent accurate in $|\Gamma|$ and 10–15° in phase before higher order modes turn on. This behavior may be due to two causes. First, when the radiated and surface waves are not weakly excited, the transmission line theory applied to the microstrip line or slotline is only an approximation, and the mode expansion approach to a certain extent involves brute force. Second, the transverse vector components (J_y and M_y), which are neglected in the present investigation, will become more important as the frequency gets higher. The VSWR's obtained by the transmission line circuit model [8] and the measurement [7] are also shown in Fig. 3 to provide a comparison. In the transmission line circuit model the stub length is assumed measured from the center of each line, and the propagation constants k_m and k_s and the excess length are obtained in the current analysis. It is seen from Figs. 3 and 4 that the present method agrees very well with the circuit model in the low-frequency range. The discrepancy for higher frequencies may be due to the higher order modes, surface waves, and radiation effects which are neglected in the circuit model. The measurements reported in [7] show wider bandwidth than that of either the circuit model or the present analysis. It is believed that the accuracy of the device parameters, the nonideal match load, and, especially, the coaxial to microstrip line transition will more or less affect the frequency-dependent results in the measurement. Besides, the material used in [7] is Custom HiK 707-20 ($\epsilon_r = 20$), which is usually very lossy especially for higher frequencies. The reasons mentioned above may explain the discrepancy between theory and experiment.

B. Slotline Discontinuities

Since the results of open-end microstrip discontinuities have been reported with the present approach in [3] and [4], they are not repeated here. However, the results by this analysis have been checked (good agreement) with the results in either [3] or [4]. Experimental results of shorted end slotline discontinuities were reported in [13]. A spectral-domain approach (SDA) of this problem has been reported in [14], where closed coplanar waveguide is used and surface wave and radiation effects are not taken into account. Slotline discontinuities with full-wave analysis have been discussed in [5], but no direct result of the equivalent circuit is provided. The shorted end resistance and reactance of a slotline are shown in Figs. 5 and 6, respectively, as a function of various device parameters. The normalized reactance obtained here is also compared with the measurements reported in [13] and the SDA method reported in [14]. The comparison shows very good agreement with the SDA method. The discrepancy with

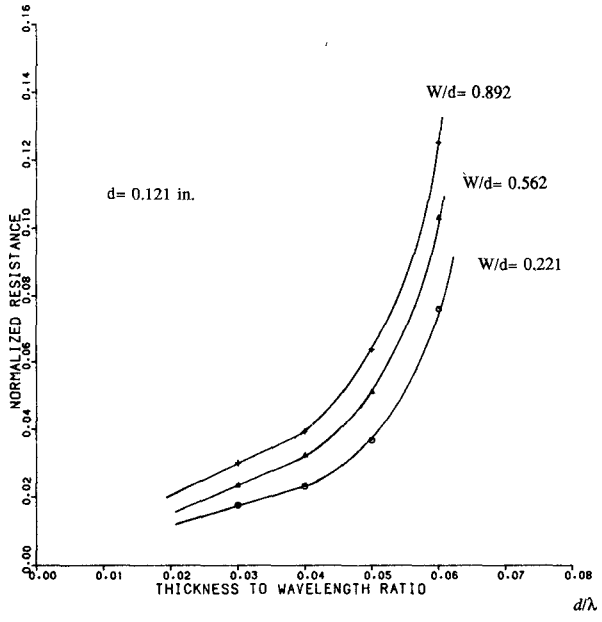

Fig. 5. Normalized end resistance of a shorted slot, $\epsilon_r = 12$.

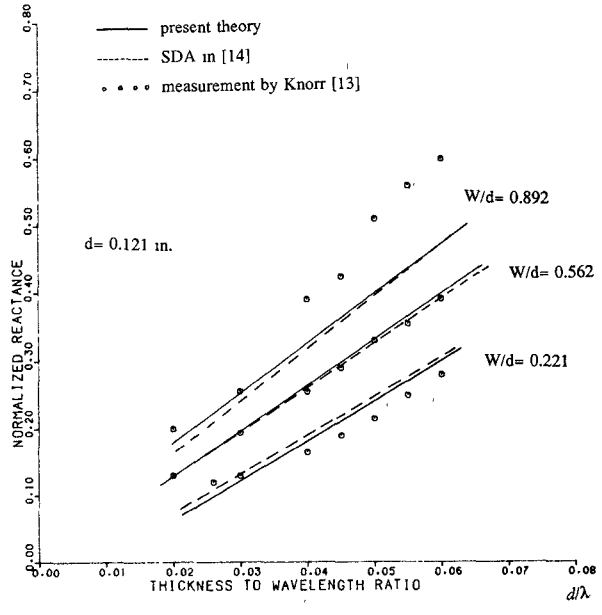

Fig. 6. Normalized end reactance of a shorted slot, $\epsilon_r = 12$.

measured results may be due to some difficulties in the measurements, as discussed in [14]. The resistance part of the equivalent circuit is due to radiation and surface waves. It is seen that the resistance increases with the increase of substrate thickness and slot width, which implies that the energy, in both surface waves and radiation, increases with substrate thickness and slot width. It is also observed that for the chosen substrate thickness ($d/\lambda_0 = 0.06$) the resistance and reactance are of the same order, which means that in this case radiated space waves and surface waves are strongly excited.

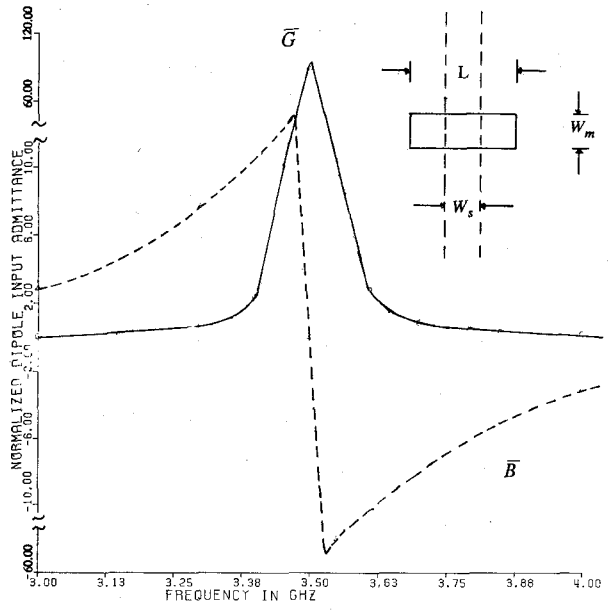

Fig. 7. Normalized equivalent admittance of a dipole fed by a slotline. $\epsilon_r = 12$, $d = 0.121$ in, $W_s = 0.562d$, $W_m = d$, and $L = 1.6$ cm.

C. A Slotline-Fed Printed Strip Dipole

In slotline circuit design, large-dielectric-constant materials are typically used to confine energy inside the material. Under this condition, the slotline is a possible candidate as a feed line of microwave or millimeter-wave printed antennas. An example of a slotline-fed printed strip dipole is shown in Fig. 7, where the input impedance of a strip dipole versus frequency is shown for $\epsilon_r = 12$ and $d = 0.121$ in. Here the input impedance does not include the tuning stub. In actual circuit design, a tuning stub is typically used to match the feed line. The results are obtained by using PWS modes on both the strip dipole and the finite but long slotline. Two δ-gap generators of the same magnitude are placed symmetrically near both ends with the dipole on the center position. Due to the symmetry, the input admittance seen at either side of the slotline is half of the input admittance of the printed strip dipole. It can be observed in Fig. 7 that resonance occurs at about 3.5 GHz. However, with a tuning stub, resonance occurs at about 3.35 GHz or at about 3.68 GHz where $\bar{G}$(normalized conductance) $= 1$. It can be seen that the bandwidth of this structure is quite small. To increase the bandwidth, the strip can be printed in low dielectric substrate while a large dielectric material is used on the other side of the ground to confine energy. One can see from Fig. 7 that when the strip dipole is off resonance, the susceptance is almost linear with frequency. This implies that strip dipole may be used as a wide-band capacitance in slotline coupler or filter design.

D. A Microstrip-Line-Fed Slot

The microstrip-line-fed slot can be used as either a radiating element or a circuit element in filter design [15]. The input impedance of a slot with a tuning stub is obtained from the information of the reflection coefficient

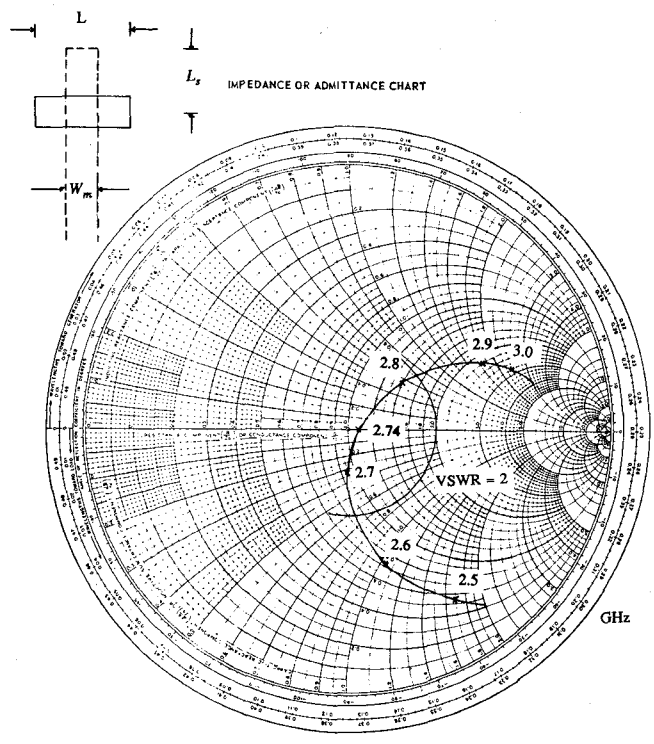

Fig. 8. Input impedance of a stub-tuned slot fed by a microstrip line. $\epsilon_r = 2.2$, $d = 0.2032$ cm, $W_m = 0.635$ cm, $W_s = 0.1016$ cm, $L = 4.0$ cm, and stub length = 0.22 cm.

in the microstrip line. The normalized input impedance of a slot fed by a microstrip as a function of frequency is plotted on the Smith chart in Fig. 8. It is seen that the bandwidth is mainly determined by the tuning stub since the resistance is quite insensitive to the frequency. Therefore to increase the bandwidth, the stub length should be chosen such that at resonant frequency the change of stub impedance with frequency is as small as possible. Another way of increasing bandwidth is to control the device parameters such that resonance occurs even without the tuning stub. Fig. 8 shows a typical example for this design where the bandwidth is about 6 percent with stub length $\approx 0.02\lambda_0$.

IV. Conclusions

A full-wave analysis is proposed in this paper to develop a generalized dynamic model for microstrip–slotline transition, microstrip-slot, and slotline-microstrip dipole, as well as slotline and microstrip discontinuities. The present approach may find some applications in other transitions in MIC design.

References

[1] K. G. Gupta, R. Garg, and I. J. Bahl, *Microstrip Lines and Slotlines*. Dedham, MA: Artech House, 1979.

[2] P. B. Katehi and N. G. Alexopoulos, "On the modeling of electromagnetic coupled microstrip antennas—The printed strip dipole," *IEEE Trans. Antennas Propagat.*, vol. AP-32, pp. 1179–1186, Nov. 1984.

[3] P. B. Katehi and N. G. Alexopoulos, "Frequency-dependent characteristics of microstrip discontinuities in millimeter wave integrated circuits," *IEEE Trans. Microwave Theory Tech.*, vol. MTT-33, pp. 1029–1035, Oct. 1985.

[4] R. W. Jackson and D. M. Pozar, "Full wave analysis of microstrip open-end and gap discontinuities," *IEEE Trans. Microwave Theory Tech.*, vol. MTT-33, pp. 1036–1042, Oct. 1985.
[5] R. W. Jackson, "Considerations in the use of coplanar waveguide for millimeter wave integrated circuits," *IEEE Trans. Microwave Theory Tech.*, vol. MTT-47, pp. 1450–1456, Dec. 1986.
[6] G. H. Robinson and J. L. Allen, "Slot line application to miniature ferrite devices," *IEEE Trans. Microwave Theory Tech.*, vol. MTT-17, pp. 1097–1101, Dec. 1969.
[7] J. B. Knorr, "Slot-line transitions," *IEEE Trans. Microwave Theory Tech.*, vol. MTT-22, pp. 548–554, May 1974.
[8] D. Chambers, S. B. Cohn, E. G. Cristol, and F. Young, "Microwave active network synthesis," Standford Resr. Inst., Semiannual Report, June 1970.
[9] N. G. Alexopoulos, D. R. Jackson, and P. B. Katehi, "Criteria for nearly omnidirectional radiation patterns for printed antennas," *IEEE Trans. Antennas Propagat.*, vol. AP-33, pp. 195–205, Feb. 1985.
[10] I. E. Rana and N. G. Alexopoulos, "Current distribution and input impedance of printed dipoles," *IEEE Trans. Antennas Propagat.*, vol. AP-29, pp. 99–106, Jan. 1981.
[11] I. E. Rana and N. G. Alexopoulos, "Correction to 'Current distribution and input impedance of printed dipoles', and 'Mutual impedance computation between printed dipoles'," *IEEE Trans. Antennas Propagat.*, vol. AP-30, p. 822, July 1982.
[12] D. M. Pozar, "Improved computational efficiency for the moment method solution of printed dipoles and patches," *Electromagnetics*, vol. 3, nos. 3–4, pp. 299–309, July–Dec. 1983.
[13] J. B. Knorr and J. Saenz, "End effect in shorted slot," *IEEE Trans. Microwave Theory Tech.*, vol. MTT-21, pp. 579–580, Sept. 1973.
[14] R. Jansen, "Hybrid mode analysis of end effects of planar microwave and millimeter wave transmission lines," *Proc. Inst. Elec. Eng.*, vol. 128, pt. H., pp. 77–86, Apr. 1981.
[15] E. A. Mariani and J. P. Agrios, "Slot-line filters and couplers," *IEEE Trans. Microwave Theory Tech.*, vol. MTT-21, pp. 1089–1095, Dec. 1970.

✠

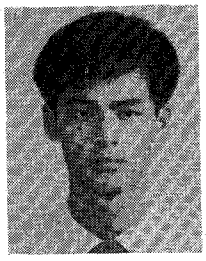

Hung-Yu Yang (S'87) was born in Taipei, Taiwan, on October 25, 1960. He received the B.S. degree in electrical engineering from National Taiwan University in 1982 and the M.S. degree in electrical engineering from the University of California at Los Angeles in 1985.

During the years 1982–1984, he served in the R.O.C. Navy as an electronics officer. He is currently working toward the Ph.D. degree at the University of California at Los Angeles. His research interests are in printed-circuit antennas and the modeling of microwave and millimeter-wave devices.

✠

Nicólaos G. Alexópoulos (S'68–M'69–SM'82–F'87) was born in Athens, Greece, in 1942. He graduated from the 8th Gymnasium of Athens and subsequently obtained the B.S.E.E., M.S.E.E., and Ph.D. degrees from the University of Michigan, Ann Arbor, in 1964, 1967, and 1968, respectively.

He is currently a Professor in the Department of Electrical Engineering at the University of California at Los Angeles, where he is also Chairman of the Electrical Engineering Department. In addition, he is a Consultant with Northrop Corporation's Advanced Systems Division. His current research interests are in electromagnetic theory as it applied to the modeling of integrated-circuit components and printed circuit antennas for microwave and millimeter-wave applications, substrate materials and their effect on integrated-circuit structures and printed antennas, inegrated-circuit antenna arrays, and antenna scattering studies.

Dr. Alexópoulos is the Associate Editor of the *Electromagnetics Journal* and *Alta Frequenza*, and he is on the Editorial Boards of the IEEE TRANSACTIONS ON MICROWAVE THEORY AND TECHNIQUES and the *International Journal on Electromagnetics Theory*.